Mesh-free simulation of complex LCD geometries

YAKUTOVICH, M. V., NEWTON, C. J. P. and CLEAVER, D. J.
<http://orcid.org/0000-0002-4278-0098>

Mesh-free simulation of complex LCD geometries.

M.V. Yakutovich[1], C.J.P. Newton[2], D.J. Cleaver[1]

[1]Materials and Engineering Research Institute, Sheffield Hallam University, Howard Street, Sheffield S1 1WB, United Kingdom

[2]Hewlett-Packard Laboratories, Filton Road, Stoke Gifford, Bristol BS12 6QZ, United Kingdom

Abstract

We use a novel mesh-free simulation approach to study the post aligned bistable nematic (PABN) cell. By employing the Qian-Sheng formalism for liquid crystals along with a smooth representation of the surface posts, we have been able to identify two distinct stable configurations. The three-dimensional order field configurations of these states and their elastic free energies are consistent with both experimental results and previous simulation attempts. However, alternative states suggested in previous studies do not appear to remain stable when finite post curvature is considered.

1 Introduction

The vast majority of liquid-crystal-based display devices rely on electro-optical differences between field-on and field-off states. Recently, though, there has been considerable interest in bistable devices [1] which possess two or more optically distinct field-off states. The utility of such devices derives from the fact that they draw power only when switching between states - once written, no power is needed to display a given pattern. In this article we concentrate on one such device – the post aligned bistable nematic (PABN) device [1]. The PABN cell shares many features with conventional LCD cells, the key difference being that one of its substrates is decorated by an array of microscopic posts, as depicted in the micrograph Fig. 1. It has been experimentally observed that a liquid crystal confined between this patterned substrate and a fixed homeotropic substrate exhibits two long-lasting field-off states, which are further referred to as planar (P) and tilted (T). It has previously been shown that appropriate control of the shapes of the surface features of this device plays a crucial role in establishing its bistability, the periodicity of these features being of lesser importance [1].

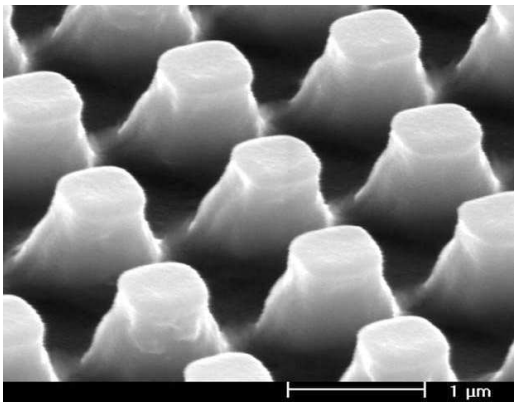

Figure 1: The PABN device [1, 2].

Here, we use a recently developed modelling approach to investigate the stable states of the PABN cell. Specifically, we apply mesh-free simulation methods to determine the 3-dimensional order tensor variation induced by its post-like substrate features. We then calculate how these change as the post shape is varied. Mesh-free methods are a promising class of numerical techniques which have been developed over the last decade as an alternative to traditional grid-based methods such as the finite difference method (FDM) and the finite element method (FEM). As their name suggests, the main idea behind mesh-free methods is that they do not rely on a grid. In certain circumstances, the ability to fully eliminate mesh creation can yield a considerable computational advantages over traditional grid-based simulation methods. In mesh-free methods, then, the spatial domain and its boundaries are represented by a set of scattered nodes with no specified inter-connectivity. As such, any confining geometry can be represented very accurately, even if the shape functions utilised are of low order. Many types of mesh-free methods have been devised so far and their different classifications are set out in the extensive reviews to be found in appropriate texts [3, 4]. Here, we employ what is termed a collocation mesh-free method. This is a truly mesh-free method which, unlike weak form methods, does not require any grid for, e.g, performing integrations. This, then, represents an extension of our previous work on the use of appropriately generalised modified smooth particle hydrodynamics methods to simulate switching behaviour in simple liquid crystal cell geometries [5].

The remainder of this article is organised as follows. In the next Section we present the Qian-Sheng description for liquid crystals which we employ in our simulations. Following this, we give a brief explanation of the framework of collocation methods with the moving least-square reproducing kernel which we have used for the shape function construction. We then proceed to describe our implementation of the PABN cell geometry and its discretisation. Finally, we demonstrate the use of these approaches for the simulation of the complex PABN cell, give an assessment of the output of these simulations and draw some conclusions.

2 Qian Sheng equations

In this section, we outline the Qian and Sheng formulation [6, 7] for a nematic liquid crystal whose orientational order is described by a $\boldsymbol{Q}$ tensor. We deliberately restrict ourselves to a description neglecting flow, since the results presented here are restricted to static arrangements. The Qian-Sheng formalism is a generalisation of Ericksen-Leslie–Parodi (ELP) theory complemented with Landau-de Gennes (LdG) theory, in which orientational order is described using the second rank, traceless, symmetric tensor $\boldsymbol{Q}$

$$Q_{\alpha\beta} = \frac{S}{2}\left(3\hat{n}_\alpha\hat{n}_\beta - \delta_{\alpha\beta}\right) + \frac{P_B}{2}\left(\hat{l}_\alpha\hat{l}_\beta - \hat{m}_\alpha\hat{m}_\beta\right). \tag{1}$$

Here, and in the remainder of this article, the tensor summation convention over repeated Greek indices is assumed. In eqn 1, these indices represent orthogonal Cartesian coordinates, while $\delta_{\alpha\beta}$ is the Kronecker delta symbol. S and P_B are the uniaxial and biaxial order parameters with $\hat{\boldsymbol{n}}$, $\hat{\boldsymbol{l}}$ and $\hat{\boldsymbol{m}}$ being orthogonal unit vectors associated with the principle axes of $\boldsymbol{Q}$. The director, $\hat{\boldsymbol{n}} = (\sin\theta\cos\phi, \sin\theta\sin\phi, \cos\theta)$, is the eigenvector corresponding to the largest eigenvalue of $\boldsymbol{Q}$. In the uniaxial approximation, $P_B = 0$ whereas in the ELP approximation, the scalar order parameter $S \to S_0$ is a constant.

The Landau-de Gennes (LdG) free energy functional [8] is defined as

$$\begin{aligned}\mathcal{F}_{Global} &= \mathcal{F}_{Bulk} + \mathcal{F}_{Surface} = \int_\Omega \{f_B\} + \int_\Gamma \{f_S\} \\ &= \int_\Omega \{f_{LdG} + f_D\} + \int_\Gamma \{f_S\},\end{aligned} \tag{2}$$

where Ω is an open-bounded set with boundary Γ, f_B is the total bulk free energy density, f_{LdG} is the LdG free energy density of the bulk, f_D is the free energy density due to elastic contributions and f_S is the surface free-energy density.

The LdG bulk free energy density $f_{LdG} \equiv f_{LdG}(\boldsymbol{Q})$ is given by an expansion in the scalar invariants of the $\boldsymbol{Q}$ tensor, truncated at the fourth-order terms:

$$\begin{aligned}f_{LdG}(\boldsymbol{Q}) &= f_{iso} + \frac{1}{2}\alpha_F Q_{\alpha\beta}Q_{\beta\alpha} - \beta_F Q_{\alpha\beta}Q_{\beta\gamma}Q_{\gamma\alpha} \\ &\quad + \gamma_F Q_{\alpha\beta}Q_{\beta\alpha}Q_{\mu\nu}Q_{\nu\mu}.\end{aligned} \tag{3}$$

Here, f_{iso} is the free energy density of the isotropic fluid, and α_F, β_F and γ_F are parameters determining the the phase of the thermotropic LC, which can be isotropic, nematic or biaxial.

The distortion free energy $f_D \equiv f_D(\partial \boldsymbol{Q})$ takes the form

$$\begin{aligned} f_D(\partial \boldsymbol{Q}) &= \frac{1}{2}L_1 \partial_\mu Q_{\nu\gamma} \partial_\mu Q_{\nu\gamma} + \frac{1}{2}L_2 \partial_\mu Q_{\nu\mu} \partial_\gamma Q_{\nu\gamma} \\ &+ \frac{1}{2}L_3 \partial_\mu Q_{\nu\gamma} \partial_\gamma Q_{\nu\mu} + \frac{1}{2}L_4 Q_{\mu\nu} \partial_\mu Q_{\gamma\tau} \partial_\nu Q_{\gamma\tau} \\ &+ \frac{4\pi L_1}{P_{ch}} \varepsilon_{\mu\nu\gamma} Q_{\mu\tau} \partial_\nu Q_{\gamma\tau} \\ &- \frac{4\pi L_4}{P_{ch}} \varepsilon_{\mu\nu\gamma} Q_{\mu\eta} Q_{\eta\tau} \partial_\nu Q_{\gamma\tau} \\ &+ \frac{6\pi^2}{P_{ch}^2} \left(L_1 Q_{\mu\nu} Q_{\nu\mu} - L_4 Q_{\mu\nu} Q_{\nu\tau} Q_{\tau\mu} \right), \end{aligned} \tag{4}$$

where $L_i,\ i = 1, \ldots, 4$ are the elastic constants and P_{ch} is the pitch of any chirality. $\varepsilon_{\alpha\beta\gamma}$ is the Levi-Civita symbol.

The central equation in the Qian-Sheng formalism, which describes the evolution of the orientational order, is

$$J\ddot{Q}_{\alpha\beta} = h_{\alpha\beta} + h^v_{\alpha\beta} - \lambda\delta_{\alpha\beta} - \varepsilon_{\alpha\beta\gamma}\lambda_\gamma, \tag{5}$$

where the superposed dot ($\dot{}$) denotes the material time derivative: $\partial_t + u_\alpha \partial_\alpha$. Here, J is the moment of inertia which is usually negligible, and we therefore set $J = 0$. λ and λ_γ are Lagrange multipliers chosen to ensure that $\boldsymbol{Q}$ remains symmetric and traceless. $\boldsymbol{h}$ is the molecular field defined by the LdG free energy as

$$h_{\alpha\beta} = -\frac{\partial f_B}{\partial Q_{\alpha\beta}} + \partial_\gamma \frac{\partial f_B}{\partial(\partial_\gamma Q_{\alpha\beta})}. \tag{6}$$

Direct calculation of the trace and off-diagonal elements of Eq. (5) shows that the Lagrange multipliers are given by $\lambda = \frac{1}{3}\left(h_{\gamma\gamma}\right)$ and $\lambda_\gamma = \frac{1}{2}\varepsilon_{\alpha\beta\gamma}h_{\alpha\beta}$.

Following [9], the equation of motion Eq. (5) can be recast in the alternative form

$$\dot{Q}_{\alpha\beta} = \frac{h_{\alpha\beta}}{\mu_1} - \frac{\lambda\delta_{\alpha\beta}}{\mu_1} - \frac{\varepsilon_{\alpha\beta\gamma}\lambda_\gamma}{\mu_1} \tag{7}$$

which is better suited to mesh-free simulation,

Finally, we state the conditions imposed on the boundaries. For infinitely strong anchoring, the $\boldsymbol{Q}$ tensor is specified according to Eq. (1). In cases of weak anchoring, however, the order tensor at the surface evolves according to

$$\mu_S \partial_t Q_{\alpha\beta} = h^S_{\alpha\beta} - \lambda^S \delta_{\alpha\beta} - \varepsilon_{\alpha\beta\gamma}\lambda^S_\gamma \tag{8}$$

where $h^S_{\alpha\beta} = -\frac{\partial f_B}{\partial\left(\partial_\tau Q_{\alpha\beta}\right)}\hat{\nu}_\tau - \frac{\partial f_S}{\partial Q_{\alpha\beta}}$, $\lambda^S = \frac{1}{3}h^S_{\gamma\gamma}$, $\lambda^S_\gamma = \frac{1}{2}\varepsilon_{\alpha\beta\gamma}h^S_{\alpha\beta}$, $\hat{\boldsymbol{\nu}}$ is an outward pointing surface unit normal vector and μ_S is the surface viscosity defined through $\mu_S = \mu_1 l_S$, where l_S is a characteristic surface length typically in the range $l_S \approx 100 - 1000$Å [10].

For planar degenerate anchoring, we use the following form for the free energy density:

$$\begin{aligned} f_S \equiv f_S(\boldsymbol{Q}) = c_1 \hat{\boldsymbol{\nu}}.Q.\hat{\boldsymbol{\nu}} + \frac{1}{2}\alpha_S Q_{\alpha\beta} Q_{\beta\alpha} \\ -\beta_S Q_{\alpha\beta} Q_{\beta\gamma} Q_{\gamma\alpha} + \gamma_S Q_{\alpha\beta} Q_{\beta\alpha} Q_{\mu\nu} Q_{\nu\mu}, \end{aligned} \tag{9}$$

where c_1 is the anchoring strength and α_S, β_S and γ_S are surface Landau coefficients.

3 The algorithm description

In this work we employ a framework of collocation mesh-free methods in which the moving least-square reproducing kernel (MLSRK) method [11, 12] is used to construct shape functions for the numerical simulation of liquid crystals. The basic idea of the collocation approach is to seek the solution of a partial differential equation on a set of independent points in space by constructing an interpolation function constructed using the values at those points.

According to the MLSRK [12] method, the approximation of a smooth field variable $f(\boldsymbol{x})$ (e.g., the Q-tensor) at some point in space $\overline{\boldsymbol{x}}$ can be given as

$$f^h(\boldsymbol{x},\overline{\boldsymbol{x}}) = \sum_{i=1}^{n} p_i(\frac{\boldsymbol{x}-\overline{\boldsymbol{x}}}{\rho})a_i(\overline{\boldsymbol{x}},\rho) = \boldsymbol{p}^T(\frac{\boldsymbol{x}-\overline{\boldsymbol{x}}}{\rho})\boldsymbol{a}(\overline{\boldsymbol{x}},\rho), \tag{10}$$

where ρ is a dilatation parameter, $\boldsymbol{p}^T(\boldsymbol{x}) = \{p_1(\boldsymbol{x}), p_2(\boldsymbol{x}), ..., p_n(\boldsymbol{x})\}$ is a vector of complete basis functions of order n and $\boldsymbol{a}^T(\overline{\boldsymbol{x}},\rho) = \{a_1(\overline{\boldsymbol{x}},\rho), a_2(\overline{\boldsymbol{x}},\rho), ..., a_n(\overline{\boldsymbol{x}},\rho)\}$ is a vector of unknown coefficients that depends on $\overline{\boldsymbol{x}}$. For example, for 3-D problems

$$\boldsymbol{p}^T(\boldsymbol{x}) = \{1, x, y, z\} \text{ for } n = 4. \tag{11}$$

These basis functions should not necessarily be polynomials, but could, alternatively, include functions which are anticipated to be present in the final solution.

The unknown coefficient vector $\boldsymbol{a}^T(\overline{\boldsymbol{x}},\rho)$ is determined by minimising the weighted squared difference with a window function $W(\boldsymbol{x}-\overline{\boldsymbol{x}},\rho)$, i.e.

$$J(\boldsymbol{a}) = \sum_{i=1}^{n} W_i(\overline{\boldsymbol{x}}-\boldsymbol{x_i},\rho)\left[\boldsymbol{p}^T(\frac{\overline{\boldsymbol{x}}-\boldsymbol{x_i}}{\rho})\boldsymbol{a}(\overline{\boldsymbol{x}}) - f_i\right]^2, \tag{12}$$

where f_i is the value of function f at the point i. By minimising the above functional, the optimal values for coefficients $\boldsymbol{a}$ are found. These ultimately lead to the following form of function interpolation:

$$f^h(\boldsymbol{x}) = \sum_{j=1}^{n} \Phi_j(\boldsymbol{x}) f_j, \tag{13}$$

where $\Phi_j(\boldsymbol{x})$ are the shape functions found using the MLSRK method.

We use the B-spline function [13] as a window function in our simulations

$$W(R,h) = \alpha_d \times \begin{cases} \frac{2}{3} - R^2 + \frac{1}{2}R^3 & 0 \le R < 1 \\ \frac{1}{6}(2-R)^3 & 1 \le R < 2 \\ 0 & R \ge 2 \end{cases} \tag{14}$$

where α_d is a normalisation factor which is equal to $3/(2\pi h^3)$ in 3-dimensions.

In order to solve the Qian-Sheng equations of Sec. 2 we additionally associate a traceless, symmetric, order tensor, $Q_{\alpha\beta}$, with each fluid particle. Microscopically, these order tensors convey information about the state of the average orientational ordering of the molecules which are assumed to be represented by each fluid particle.

The resulting simulation algorithm centres, then, on solving the set of Qian-Sheng eqns. (7, 8), which are already written in the strong form, on a set of randomly distributed points. Particles are given initial values of Q. Then, eqns. (7, 8) are considered for each particle, with their right-hand sides replaced by the appropriate kernel estimates. We adopt a simple two step predictor-corrector scheme to integrate the resulting linear ordinary differential equations to second order accuracy.

4 Geometry

In order to represent the geometry of the PABN device's patterned substrate in a smooth fashion, we impose periodic boundary conditions in x and y and use the following surface to describe the height of a single post as a function of x and y:

$$f(x,y) = \tanh\left(\pi\left(sx-p\right) - \tanh\left(\pi\left(sx+p\right)\right)\right) \times$$
$$\tanh\left(\pi\left(sy-p\right)\right) - \tanh\left(\pi\left(sy+p\right)\right). \tag{15}$$

Here p controls the post's width and length and s gives the smoothness of the whole structure. An example of a such function is given in Figure 2(a). This geometry is given on the interval $[-1:1]$ in the x and y dimensions and has unit height. Thus, it can easily be scaled to represent any dimensions.

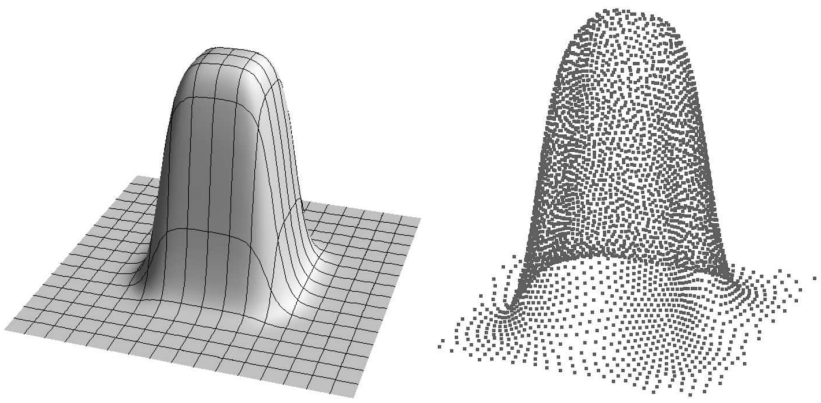

(a) An example of the analytical shape of the post structure.

(b) An example of discretisation using Monte-Carlo technique.

Figure 2: Post structure used in simulations.

The biggest advantage of such a representation is the absence of any sharp corners. This effectively prevents development of unphysical defects in the system. Another advantage comes from the fact that we can both closely represent the geometry and, at the same time, precisely know the normal at each point on the surface. Thus, the numerical calculation of planar anchoring is more accurate than that achieved, e.g., with traditional grid-based methods.

Within our main simulations, the smooth surface eqn (15) was actually represented by a number of discrete points residing on that surface. Having attempted a number of analytical routes for setting these surface points, and failed to find one that reliably avoided undesirable clustering behaviours, we have implemented a Monte-Carlo-based numerical approach instead. Within this, the surface was gradually loaded with interaction sites, which were able to rearrange themselves (by standard Monte Carlo moves) across the surface, subject to Lennard-Jones like interactions which promote a particular inter-point spacing. Indeed, by allowing this natural spacing to vary slightly across the surface, we found it straightforward to achieve the desirable outcome of having higher surface-point densities in high curvature regions of the surfaces (i.e. at the post edges and corners). In practice, the final surface point distribution was taken as that achieved when no more points could be introduced and the total interaction energy had equilibrated. An example of this discretisation is given in Fig. 2(b).

5 Modelling

In this Section, we present the results obtained from application of our mesh-free Qian Sheng simulation approach to the PABN system. Within this, we make repeated reference to a previous modelling study of this device by Majumdar et al [2]. It should be noted, however, that in [2] the post was represented as a rectangular box, whereas we employ the smooth three-dimensional shape depicted in the Fig. 2. Consequently, we do not have to prescribe the liquid crystal orientation at the edges of the post, which ultimately helps us to avoid possible unphysical artifacts. Further, since features such as edge defect lines are not pinned in our simulations, the equilibrated systems are not required to possess the same topologies as the initial configurations.

All of our simulations were initiated to one of a set of trial configurations from which the system was allowed to relax into a local free energy minimum. The initial trial configurations used were constructed in a similar way to those described in [2]. Explicitly, each particle Q tensor was set such that the principal direction of the order tensor followed a specified vector field $\boldsymbol{n} = \{n_x, n_y, n_z\}$ whose non-normalised components are given below.

In all trial configurations, the x and y components of the vector $\boldsymbol{n}$ were given by

$$\begin{aligned} n_x &= \left[\sin\left(\frac{\pi x}{L_p}\right)\right]\left(\frac{H-z}{H}\right), \\ n_y &= \left[\sin\left(\frac{\pi y}{L_p}\right)\right]\left(\frac{H-z}{H}\right), \end{aligned} \tag{16}$$

where H is the cell height and L_p the post's cross-sectional dimension. For particles above the top of post (height h), the z-component of $\boldsymbol{n}$ was also the same for all trial configurations and given by

$$n_z = \frac{z-h}{H-h}. \tag{17}$$

Four different configurations were considered for the z-component of the vector $\boldsymbol{n}$ for particles below the top of the post. These were given by

$$n_z = \begin{cases} z(h-z), & T, \\ z(h-z)\left[1+\cos\left(\frac{\pi x}{L_p}\right)+\cos\left(\frac{\pi y}{L_p}\right)\right], & P_1, \\ z(h-z)\cos\left(\frac{\pi x}{L_p}\right), & P_2, \\ z(h-z)\cos\left(\frac{\pi x}{L_p}\right)\cos\left(\frac{\pi y}{L_p}\right), & P_3. \end{cases}$$

where the labels T and P denote tilted and planar states. These four arrangements correspond to the distinct arrangements identified from the finite element simulations presented in [2]

The simulations we have performed using these 4 different initial configurations have equilibrated to only two stable configurations – T and P_1. In comparison, the finite element simulations presented in [2] found distinct energy minima for all four configurations. All of the simulations that we have initiated with P_3 and P_4 initial configurations have converted into the tilted state T, which we have found to be the state with the lowest free energy. These interconversion simulations have all involved the depinning of highly distorted regions from the post faces and, ultimately, topological changes. In contrast, the continued stability of the P_1 arrangement suggests it as the most plausible arrangement for the experimentally observed planar state. Below we describe the observed states P_1 and T in more detail.

First, we consider the tilted state, T. Experimentally, PABN cells cooled from the isotropic liquid crystal phase always adopt this state [1]. Our simulations are consistent with this observation since we find that this state is adopted from a wide range of starting configurations and topologies. We show a slice through the tilt state order field obtained from our simulations in Fig. 3. This is a periodic cross-section taken along the post diagonal. Between the posts, this shows a relatively rapid rearrangement from planar to near-vertical. but little elastic distortion above that. The other significant distortions associated with the tilt state are topological in nature. As shown in Fig. 4, which shows the order field around a single post from a slightly oblique value, the state contains two defects – one at the base of the leading edge and a second at the top of the trailing corner.

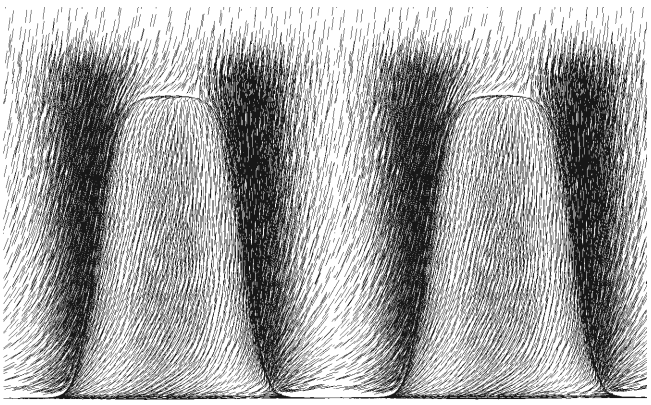

Figure 3: Periodic cross-section of the tilted state T along the post diagonal.

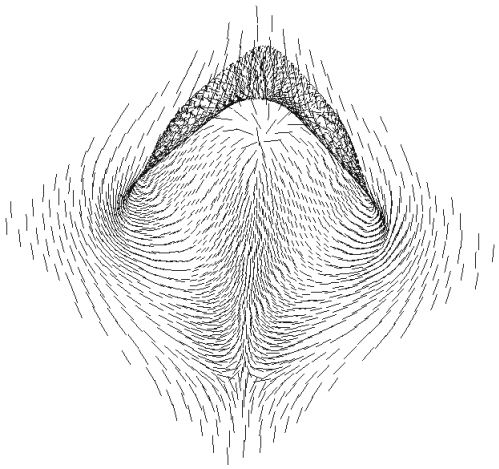

Figure 4: Near-top-down view of the equilibrated tilt state in the region of a single post, showing defects at the base of the leading corner and the top of the trailing corner.

In the planar configuration P_1, the order field cross-section across the post diagonals was found to take the form depicted in Fig. 5. Here, the liquid crystal director adopts an asymmetrical U-shape profile between the posts. This asymmetry derives from the differences in the configurations adopted at the leading and trailing faces. This finding is in qualitative agreement with the topological and configurational results provided in [2]. In this state, we observe a small degree of biaxiality adjacent to the post's leading and trailing edges, the value of which does not exceed 0.05. This biaxiality has been predicted in earlier works [1] but was not found in the finite element simulation of [2].

As well as observing these topological and orientational differences between the T and P_1 states, we have also performed an initial quantitative comparison of their elastic deformation energies. For all post shapes considered thus far, these calculations show that the tilt state is the more stable. These calculations are

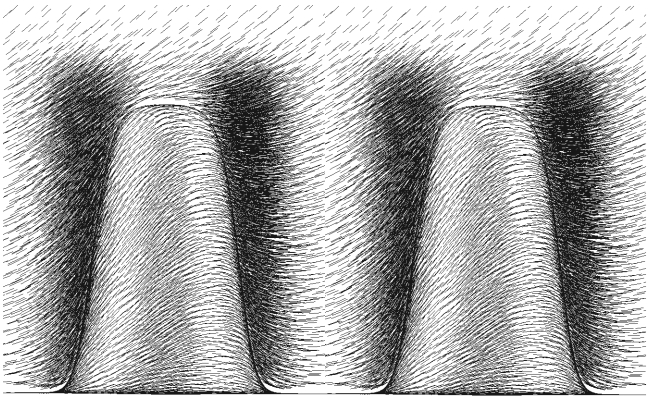

Figure 5: Periodic cross-section of the planar state P_1 across posts' diagonals.

summarised by the data shown in Fig. 6 which show how the elastic free energies of the two states varies with post height h. The trend shown here, approximately linear variation with h for each state, is in qualitative agreement with previous findings [2].

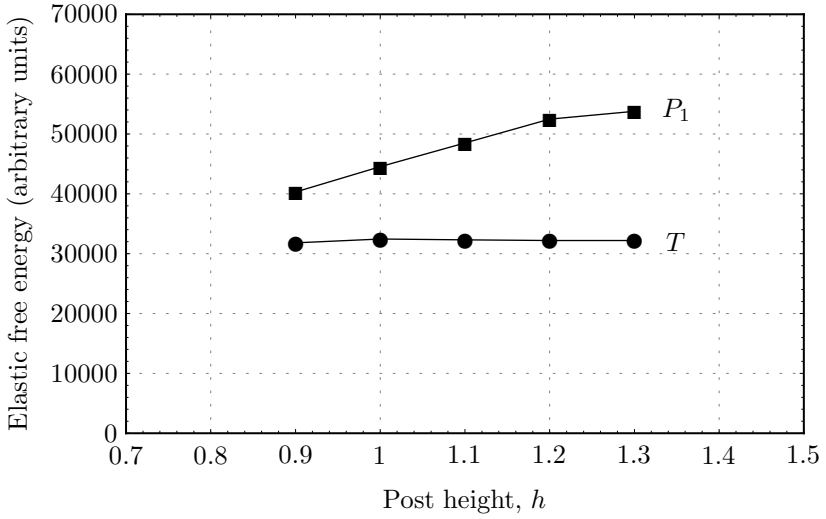

Figure 6: Elastic free energies of different states as a function of post height.

6 Conclusion

In this paper, we have used a novel mesh-free simulation method to model the equilibrium states of the bistable PABN cell. In this, we have employed a truly mesh-free collocation technique based on the moving least-square reproducing kernel method. This has enabled us to execute simulations based on the Qian-Sheng Q-tensor formalism in geometries involving complex three-dimensional smooth substrates. This approach has allowed us to include spatially variable nematic order parameter and biaxiality as simulation observables. Further, since it allows topological changes to take place, the method is able to escape from globally unstable

configurations. From our simulations, we have found two distinct stable configurations which qualitatively agree with the tilted and planar arrangements seen experimentally. The elastic free energies calculated for these states qualitatively agree with previous simulation work.

In future work, we intend to extend our study by assessing the dynamical behaviour of the PABN switching between two stable states. This will require a full nematodynamic description of the liquid crystal cell. Further, a full electric field solver and flexoelectric terms in the governing equations will be incorporated.

7 Acknowledgements

MY acknowledges financial support from Sheffield Hallam University and Hewlett-Packard Laboratories. This work has benefitted from discussions with Chris Care and Tim Spencer.

References

[1] S. Kitson and A. Geisow. Controllable alignment of nematic liquid crystals around microscopic posts: Stabilization of multiple states. *Applied Physics Letters*, 80(19):3635–3637, MAY 13 2002.

[2] A. Majumdar, C. J. P. Newton, J. M. Robbins, and M. Zyskin. Topology and bistability in liquid crystal devices. *Physical Review E*, 75(5):051703, MAY 2007.

[3] G. R. Liu. *Mesh Free Methods: Moving Beyond the Finite Element Method*. CRC Press Inc, 2002.

[4] Li Shaofan and Kam Wing Liu. *Meshfree Particle Methods*. Springer-Verlag Berlin, 2004.

[5] M. V. Yakutovich, C. M. Care, and D. J. Cleaver. Mesh-free modelling of liquid crystals using modified smoothed particle hydrodynamics. 2008. Submitted.

[6] T. Z. Qian and P. Sheng. Generalized hydrodynamic equations for nematic liquid crystals. *Physical Review E*, 58(6):7475–7485, DEC 1998.

[7] T. J. Spencer and C. M. Care. Lattice boltzman scheme for modeling liquid-crystal dynamics: zenithal bistable. *Physical Review E*, 74(6), 2006.

[8] P. G. De Gennes and J. Frost. *The Physics of Liquid Crystals*. Clarendon press, Oxford, 2nd edition, 1993.

[9] C. M. Care, I. Halliday, and K. Good. Lattice boltzmann nemato-dynamics. *Journal of Physics-Condensed Matter*, 12(43):L665–L671, OCT 30 2000.

[10] M. Vilfan, I. D. Olenik, A. Mertelj, and M. Copic. Aging of surface anchoring and surface viscosity of a nematic liquid crystal on photoaligning poly-(vinyl-cinnamate). *Physical Review E*, 63(6):061709, JUN 2001.

[11] T. Belytschko, Y. Krongauz, D. Organ, M. Fleming, and P. Krysl. Meshless methods: An overview and recent developments. *Computer Methods in Applied Mechanics and Engineering*, 139(1-4):3–47, DEC 15 1996.

[12] W. K. Liu, S. F. Li, and T. Belytschko. Moving least-square reproducing kernel methods .1. methodology and convergence. *Computer Methods in Applied Mechanics and Engineering*, 143(1-2):113–154, APR 15 1997.

[13] J. J. Monaghan and J. C. Lattanzio. A refined particle method for astrophysical problems. *Astronomy and Astrophysics*, 149(1):135–143, 1985.